Plant nanobionics approach to augment photosynthesis and biochemical sensing

Juan Pablo Giraldo[1], Markita P. Landry[1], Sean M. Faltermeier[1], Thomas P. McNicholas[1], Nicole M. Iverson[1], Ardemis A. Boghossian[1,2], Nigel F. Reuel[1], Andrew J. Hilmer[1], Fatih Sen[1,3], Jacqueline A. Brew[1] and Michael S. Strano[1]*

The interface between plant organelles and non-biological nanostructures has the potential to impart organelles with new and enhanced functions. Here, we show that single-walled carbon nanotubes (SWNTs) passively transport and irreversibly localize within the lipid envelope of extracted plant chloroplasts, promote over three times higher photosynthetic activity than that of controls, and enhance maximum electron transport rates. The SWNT–chloroplast assemblies also enable higher rates of leaf electron transport *in vivo* through a mechanism consistent with augmented photoabsorption. Concentrations of reactive oxygen species inside extracted chloroplasts are significantly suppressed by delivering poly(acrylic acid)–nanoceria or SWNT–nanoceria complexes. Moreover, we show that SWNTs enable near-infrared fluorescence monitoring of nitric oxide both *ex vivo* and *in vivo*, thus demonstrating that a plant can be augmented to function as a photonic chemical sensor. Nanobionics engineering of plant function may contribute to the development of biomimetic materials for light-harvesting and biochemical detection with regenerative properties and enhanced efficiency.

Chloroplasts are the ultimate source of chemical energy in food supplies and carbon-based fuels on the planet. By capturing atmospheric CO_2, these plant organelles convert light energy into three major forms of sugars that fuel plant growth: maltose, triose phosphate, and glucose[1]. Whereas photosystems interfaced with nanomaterials are extensively studied, nanoengineering chloroplast photosynthesis for enhancing solar energy harnessing remains unexplored[2]. One major deterrent in using chloroplast photosynthetic power as an alternative energy source is that these organelles are no longer independently living organisms. However, isolated chloroplasts from the algae *Vaucheria litorea* in symbiotic association with the sea slug *Elysia chlorotica* remarkably remain functional for at least 9 months[3,4]. Land plant chloroplast photosystem activity declines within a day after extraction[5,6], and *ex vivo* sugar output has been reported for only a few hours[1,7]. Although chloroplasts have mechanisms in place to self-repair photodamaged proteins[8], as well as a double-stranded circular DNA with a subset of protein-encoding genes involved in photosynthesis[9], and ribosomal units for protein synthesis and assembly[10], little is known about engineering these plant organelles for long-term, stable photosynthesis *ex vivo*. Another limitation of chloroplast photosynthesis is that absorbed light is constrained to the visible range of the spectrum, allowing access to only roughly 50% of the incident solar energy radiation[11]. Furthermore, less than 10% of full sunlight saturates the capacity of the photosynthetic apparatus[12]. Photosynthetic organisms evolved for reproductive success, including shading competitors, not solely for solar energy conversion efficiency. Thus, improving photosynthetic efficiency may require extending the range of solar light absorption[13], particularly in the near-infrared spectral range, which is able to penetrate deeper into living organisms.

The high stability and unique chemical and physical traits of nanomaterials have the potential to enable chloroplast-based photocatalytic complexes both *ex vivo* and *in vivo* with enhanced and new functional properties. SWNTs embedded within chloroplasts have the potential to enhance the light reactions of photosynthesis with their distinctive optical and electronic properties. Under bright sunlight, chloroplast photosystems capture more photons than they can convert into electron flow[14]. However, under non-saturating light conditions, maximizing solar energy capture is crucial[15]. SWNTs absorb light over a broad range of wavelengths in the ultraviolet, visible and near-infrared spectra not captured by the chloroplast antenna pigments. The electronic bandgap of semiconducting SWNTs allows them to convert this absorbed solar energy into excitons[16] that could transfer electrons to the photosynthetic machinery. Also, SWNT-based nanosensors can monitor single-molecule dynamics[17] of free radicals within chloroplasts for optimizing photosynthetic environmental conditions (light and CO_2). However, nanoengineering photosynthesis requires the delivery of nanomaterials through the chloroplast outer envelope. Nanoparticle transport through lipid bilayers has been described to be energy dependent, requiring endocytosis pathways[18] that have not been reported in isolated chloroplasts. So far, nanomaterial uptake mechanisms through cell membranes are controversial[19] and poorly understood in organelles such as chloroplasts.

Cerium oxide nanoparticles (nanoceria) also have been demonstrated to catalyse the quenching of reative oxygen species (ROS) in retinal cells, significantly reducing their intracellular concentrations[20]. Chloroplasts have natural biochemical pathways to scavenge ROS and mechanisms for photosystem protein self-repair[8]. However, most enzymes involved cannot be synthesized *ex vivo* because they lack the polypeptide precursors imported from the plant cell cytosol[21]. Technologies that localize nanoceria at the sites of ROS generation can exploit the oxygen vacancies in the CeO_2 lattice structure to effectively trap free radicals before

[1]Department of Chemical Engineering, Massachusetts Institute of Technology, Cambridge, Massachusetts 02139, USA, [2]Department of Chemical Engineering, California Institute of Technology, Pasadena, California 91125, USA, [3]Department of Biochemistry, Dumlupinar University, Kutahya 43020, Turkey. *e-mail: strano@mit.edu
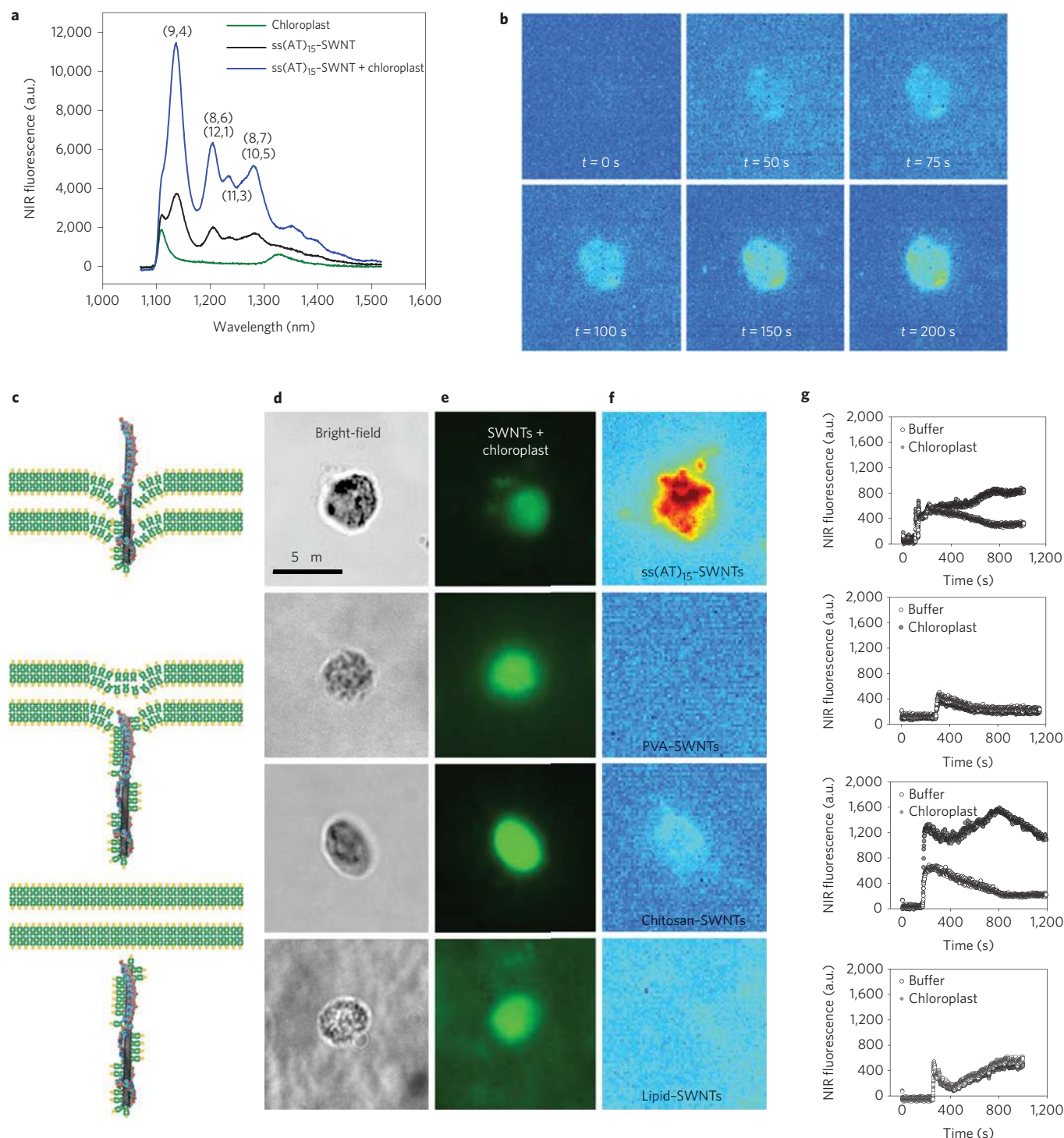
Figure 1 | Mechanism of SWNT trapping by chloroplast lipid bilayers. a, Chloroplast autofluorescence was masked from near-infrared images by a long-pass 1,100 nm filter. **b**, Near-infrared photo still indicating rapid penetration of ss(AT)₁₅–SWNTs through the lipid bilayers of isolated chloroplasts. **c**, SWNT transport through chloroplast double membrane envelope via kinetic trapping by lipid exchange. **d–f**, Bright-field (×100; **d**) and near-infrared (×100; **e**) images of isolated chloroplasts indicating uptake of SWNTs coated in ss(AT)₁₅ DNA and chitosan, but not of PVA- and lipid-coated SWNTs (×100; **f**). **g**, Change in average SWNT fluorescence in cross-sections of chloroplasts versus external buffer solution. Laser excitation 785 nm at 75 μW.

they damage nearby pigments, reaction centres and photosynthetic proteins. We have recently shown that cerium leakage, from dextran nanoceria particles not able to penetrate the chloroplast outer envelope, promotes only minor scavenging of photogenerated ROS (ref. 2). Thus, we predicted far more effective catalytic ROS

scavenging and extended chloroplast photosynthetic activity by assembling nanoceria within the photosynthetic machinery.

In this work, we develop a concept that is heretofore unexplored in the literature. We examine whether and how nanomaterials can interface specifically with plant organelles *ex vivo* and *in vivo* to
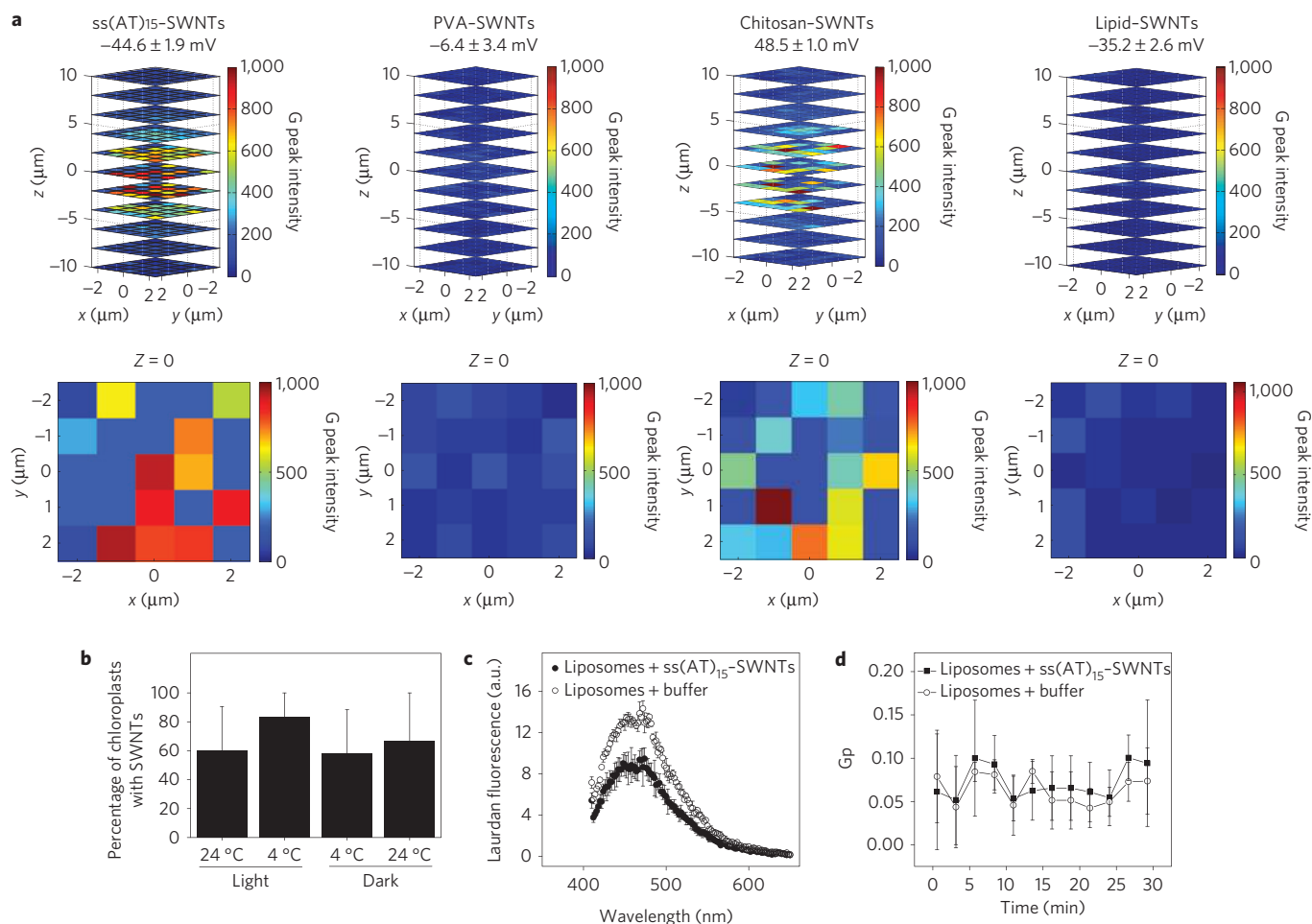
Figure 2 | The ss(AT)$_{15}$–SWNT lipid exchange with the chloroplasts' outer envelope via a passive uptake mechanism is dependent on zeta potential. **a**, Confocal Raman spectroscopy 3D maps localized ss(AT)$_{15}$ and chitosan SWNTs inside chloroplasts whereas relatively neutral PVA and lipid SWNTs were not present. Chloroplasts were approximately 5 μm in diameter and centred at $Z = 0$. Values correspond to SWNT G-band intensity (1,580 cm^{-1}) under a laser excitation of 658 nm at 145 μW. **b**, Average percentage of chloroplasts with SWNTs is not influenced by light or temperature conditions. **c,d**, ss(AT)$_{15}$–SWNTs quench laurdan fluorescence in DGDG and MGDG liposomes (**c**), but do not modify laurdan generalized polarization (Gp), an indicator of membrane fluidity (**d**). Error bars represent s.d. ($n = 3$).

enable new or enhanced functions. We reason that the assembly of nanoparticle complexes within the chloroplast photosynthetic machinery has the potential to enhance solar energy conversion through augmented light reactions of photosynthesis and ROS scavenging while imparting new sensing capabilities to living plants. This effort is divided into objectives that attempt to understand a newfound mechanism of transport and spontaneous assembly of nanomaterials inside chloroplasts; increase the photosynthetic activity in chloroplasts through specific nanoparticle assemblies within photosynthetic machinery; enhance the ability of the chloroplast to scavenge ROS using cerium and carbon-based nanoparticles transported to optimal sites of ROS generation; and enable real-time monitoring of free-radical species and environmental pollutants using *in vivo* and *ex vivo* embedded nanosensors. These objectives constitute a plant nanobionics approach to generating new constructs for bionanotechnology research, which may contribute to biomimetic energy generation and the creation of new plant biochemical detectors.

Nanoparticle spontaneous assembly within chloroplasts

We used single-particle tracking of near-infrared fluorescent semiconducting SWNTs to investigate their interaction with isolated plant chloroplasts from spinach leaves. SWNTs do not photobleach and fluoresce in the near-infrared region above 1,100 nm, where chloroplast autofluorescence is minimal (Fig. 1a). SWNT fluorescence of chiralities (9,4), (8,6), (12,1), (11,3), (8,7) and (10,5) was quantified inside chloroplasts using a laser excitation (785 nm) that is off-resonance to photosynthetic pigments. Surprisingly, SWNTs suspended in strongly cationic or anionic coatings (that is, high magnitude of the zeta potential) were found to traverse and localize rapidly within the chloroplast outer envelope and not just adsorb to the exterior. The process is observed to occur within seconds of nanoparticle interaction with the inner and outer lipid bilayer (Fig. 1b). This process is irreversible, and in the case of ss(AT)$_{15}$ DNA- and chitosan-coated SWNTs dosed at 2.5 mg l^{-1} concentration, leaves no free nanotubes suspended in the buffer solution (Supplementary Video).

Not all SWNT types are transported through lipid bilayers. Both near-infrared SWNT fluorescent images (Fig. 1d–g) and confocal three-dimensional (3D) mapping of the characteristic SWNT Raman G-band (1,580 cm^{-1}) (Fig. 2a) indicate that whereas ss(AT)$_{15}$ and chitosan SWNTs are embedded within chloroplasts, polyvinyl alcohol (PVA)- and lipid-coated SWNTs do not interact with the lipid bilayer. Thus, we confirmed modelling
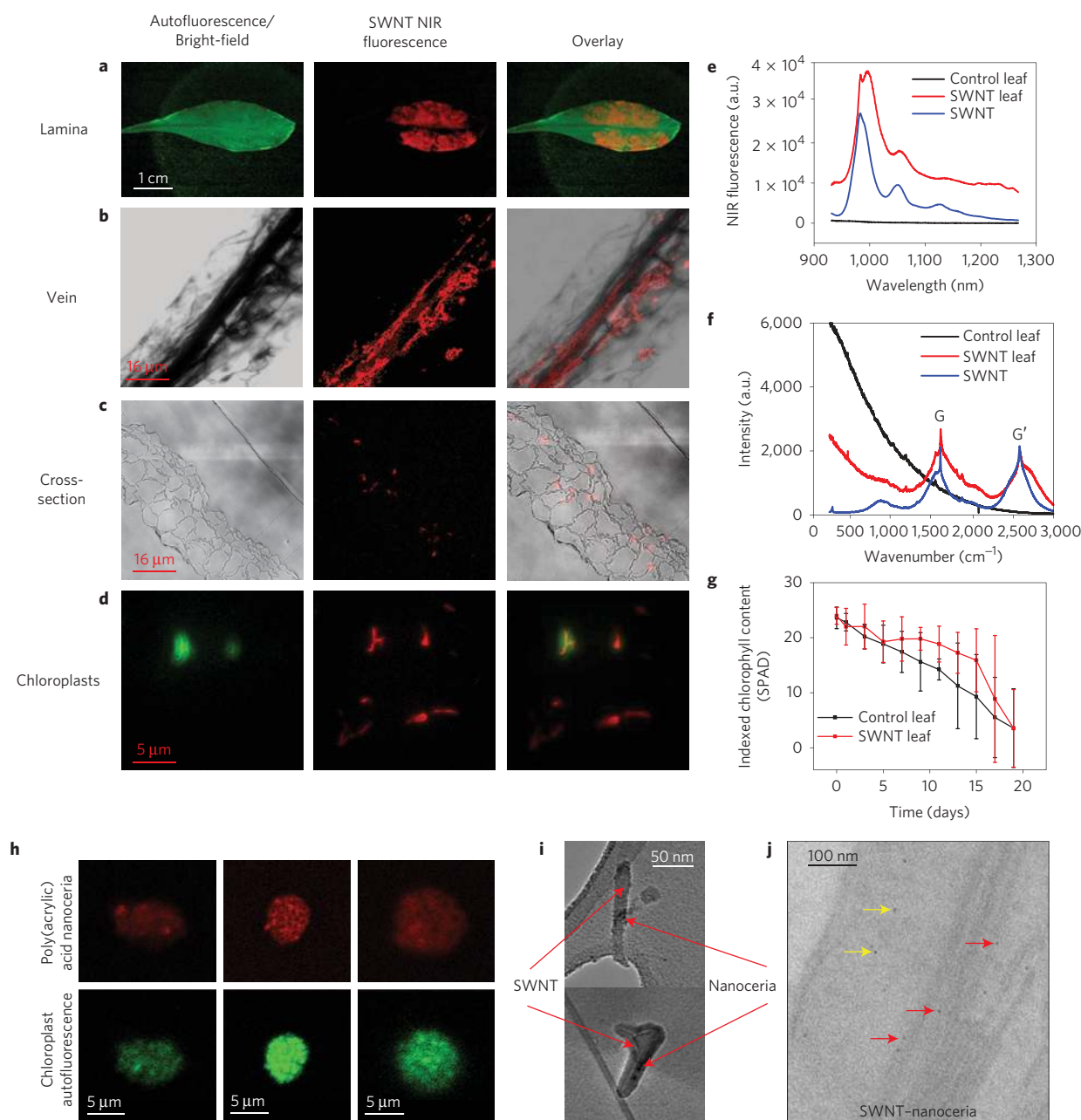
Figure 3 | Nanoparticle transport inside isolated chloroplasts and leaves. a, CRi Maestro images of ss(AT)$_{15}$–SWNTs within the leaf lamina of *A. thaliana*. **b–d**, Co-localization of ss(AT)$_{15}$–SWNTs near leaf veins (×20; **b**), in parenchyma cells (×20; **c**) and chloroplasts *in vivo* (×63; **d**). **e**, Near-infrared fluorescence signal of SWNTs in leaves relative to SWNTs in solution. **f**, Raman spectroscopy showed broadening of G and G′ SWNT peaks in leaves. **g**, Temporal patterns of chlorophyll content indicated similar lifespans for leaves with SWNTs and controls. Error bars represent s.d. (*n*=4). **h**, Confocal images of chloroplasts assembled with PAA–NC: chlorophyll (green) co-localized with PAA–NC labelled with Alexa Fluor 405 (red). **i**, TEM images of the SWNT–NC complex. **j**, Chloroplast TEM cross-section after incubation in SWNT–NC suspension. Nanoparticles localized both in the chloroplasts' thylakoid membranes (red arrows) and the stroma (yellow arrows). Elemental analysis by ICP-MS of chloroplasts with the SWNT–NC complex detected the presence of cerium at 95±0.1 ppm.

studies identifying SWNT surface patterning and charge as key traits determining penetration through lipid membranes[19,22]. A highly negative or positive SWNT zeta potential favours nanotube adsorption to the chloroplast lipid membrane (Fig. 2a). The ss(AT)$_{15}$ and chitosan SWNTs, having zeta potentials of −44.6±1.9 mV and 48.5±1.0 mV, respectively, are transported inside chloroplasts but not PVA-coated SWNTs with more neutral values, −6.4±3.4 mV. However, lipid–SWNTs with a negative zeta potential, −35.2±2.6 mV, are unable to move through the chloroplast outer envelope, confirming membrane trapping inhibition once SWNTs are coated with lipids.

SWNT movement through chloroplast membranes occurs via passive mechanisms. Neither variation in temperature from 4° to 24 °C nor light conditions influenced chloroplast ss(AT)$_{15}$– SWNT uptake (Fig. 2b). Previous studies of protein transport inside chloroplasts have used temperature as an indicator of metabolic activity and light conditions as a proxy for ATP generation[23]. Together these results suggest that SWNTs are transported through
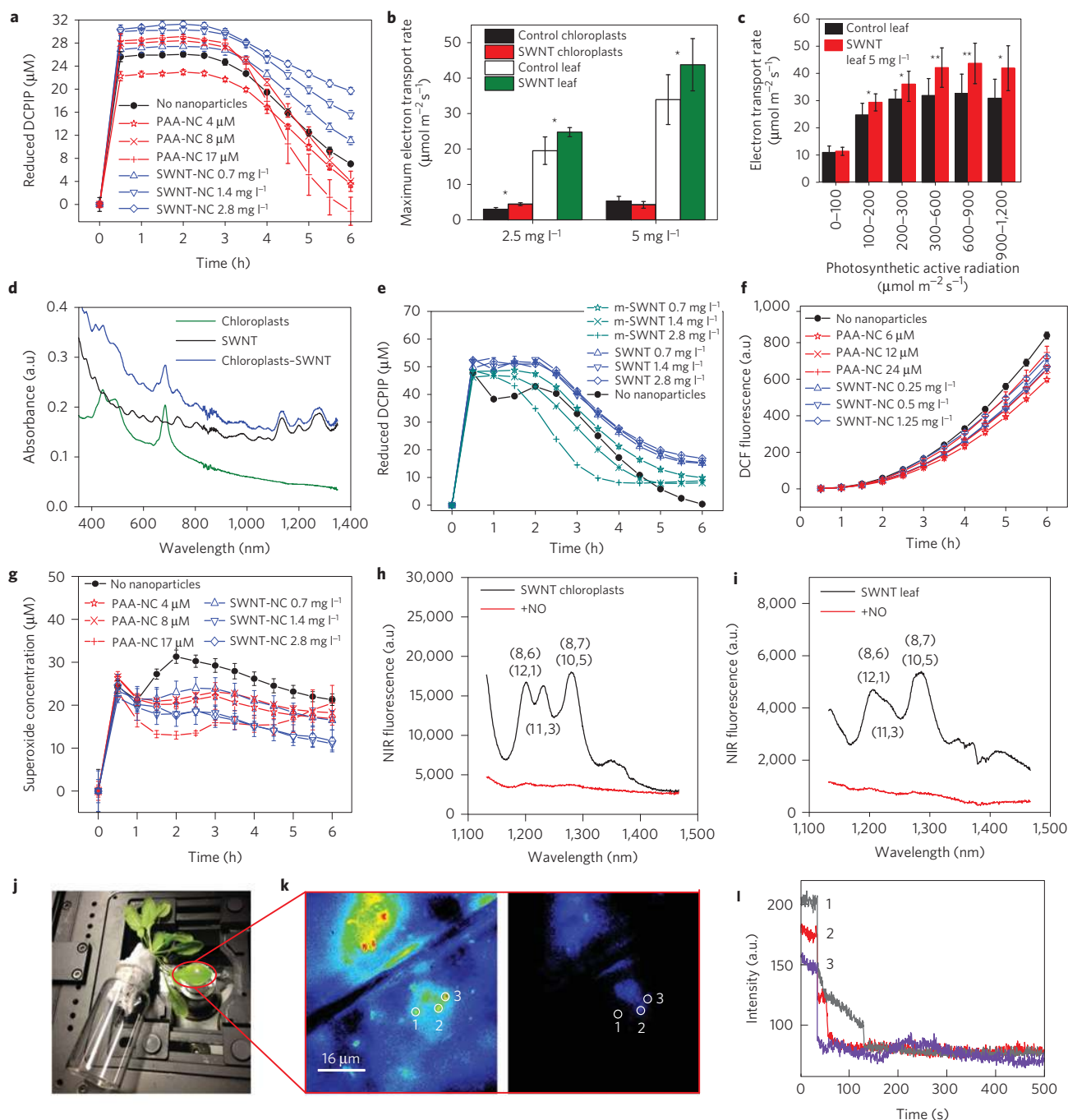
Figure 4 | SWNT and nanoceria plant nanobionics. a, Enhanced photosynthetic activity of isolated chloroplasts with SWNT–NC was shown by electron transfer to DCPIP. **b**, Higher maximum electron-transport rates in extracted chloroplasts and leaves were quantified by the yield of chlorophyll fluorescence ($P < 0.05$, t-test, $n = 3$–8). **c**, Electron-transport-rate light curves indicated enhanced photosynthesis above 100 µmol m^{-2} s^{-1} for 5 mg l^{-1} SWNT leaves ($P < 0.05$, t-test, $n = 5$–8). **d**, SWNTs modified chloroplast ultraviolet, visible and near-infrared absorption spectrum. **e**, A suspension made mostly of semiconducting SWNTs increased chloroplast reduction of DCPIP whereas a solution enriched with metallic SWNTs (m-SWNTs) had lower effect in photosynthetic activity. **f**, Increased ROS scavenging by SWNT–NC and PAA–NC inside chloroplasts was quantified by the oxidation of H$_2$DCFDA to DCF. **g**, Reduction in superoxide concentration was facilitated by nanoparticles localized at chloroplast sites of ROS generation. **h,i**, NO sensing by ss(AT)$_{15}$–SWNTs delivered into extracted chloroplasts (**h**) and *in vivo* in leaves of *A. thaliana* (**i**) was evidenced by a strong quenching in fluorescence for all chiralities. **j**, *In vivo* plant sensing set-up whereby a leaf infiltrated with ss(AT)$_{15}$–SWNTs was excited by a 785 nm epifluorescence microscope. **k**, ×20 view of ss(AT)$_{15}$–SWNTs inside a leaf before (left) and after (right) addition of 20 µl dissolved NO solution with three SWNT regions of interest circled. **l**, Peak intensity–time traces of three ss(AT)$_{15}$–SWNT regions showed stepwise quenching of SWNT by NO, ranging from 40 to 60% intensity decrease. Error bars represent s.d.

the chloroplast membranes in a process driven by diffusion and spontaneous surface reaction. Consistent with our results, it has been reporte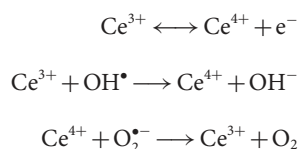d that carboxylated SWNTs localize in mitochondria[24], an organelle lacking endocytic pathways. The adsorption of chloroplast lipids on the SWNT surface occurs without a shift in laurdan fluorescence, an indicator of membrane fluidity (Fig. 2c,d).

However, laurdan fluorescence quenching points to an interaction of the fluorophore with membrane-bound SWNTs.

We propose that SWNT penetration through the chloroplast lipid bilayer occurs via kinetic trapping by lipid exchange (Fig. 1c). Glycerolipids, forming most of the chloroplast outer envelope (2.5–3 mg of lipids per milligram of protein; ref. 25), wrap around SWNTs as they interact with the membrane. The disruption of the chloroplast membranes leads to lipid adsorption to the hydrophobic SWNT surface. As nanotubes penetrate through the envelopes, they are coated with a layer of lipids that irreversibly binds them to the chloroplast interior. The lipid membrane re-heals after the nanoparticle uptake process is completed. This nanoparticle-enabled uptake mechanism through lipid bilayers is a new pathway for material delivery into plant organelles.

The ss(AT)$_{15}$–SWNTs were also delivered to chloroplasts of *Arabidopsis thaliana* leaves *in vivo* by infiltration through the leaf lamina (Fig. 3a–d and Supplementary Fig. 1a–d). Leaves assembled with CoMoCAT ss(AT)$_{15}$–SWNTs (SouthWest NanoTechnologies) showed a characteristic fluorescence peak for the (6,5) chirality (980–1,000 nm) throughout the lamina in both CRi Maestro images and the near-infrared spectrum (Fig. 3a,e). A sharp peak shoulder in SWNT leaf near-infrared fluorescence was attributed to the Raman scattering in carbon nanotubes. The Raman spectra of ss(AT)$_{15}$–SWNTs inside leaves was similar to nanoparticles in suspension except for a broadening of the G and G' bands (Fig. 3f). SWNTs have been previously shown to penetrate cell walls and membranes of tobacco cell cultures[26]. By imaging leaf tissue cross-sections, SWeNT SG76 ss(AT)$_{15}$–SWNTs (SouthWest NanoTechnologies) were localized to the leaf veins and both in intracellular and extracellular parenchyma tissues (Fig. 3b,c), indicating transport through leaf cell membranes and walls. Co-localization images of chloroplast and near-infrared SWNT fluorescence indicated that SWNTs were associated with chloroplasts inside parenchyma cells (Fig. 3d). No SWNT near-infrared fluorescence was detected in control leaves treated with only infiltration medium (Supplementary Fig. 1a–d). Leaf lifespan was not affected by infiltration with ss(AT)$_{15}$–SWNTs at 5 mg l^{-1} (Fig. 3g). Leaf chlorophyll content has been used as a proxy for indicating the timing of leaf senescence, a type of programmed cell death in which the photosynthetic machinery is dismantled[27]. Both SWNT leaves and control leaves treated with infiltration medium showed similar temporal patterns in chlorophyll content for 20 days until the end of leaf lifespan.

A compelling application of this spontaneous transport and assembly of SWNTs within the chloroplast is to localize other nanoparticles within the envelope and ultimately on the thylakoid membranes. Nanoceria are one of the most potent reactive oxygen scavengers available and have the potential to significantly reduce ROS generation at the sites of generation. However, no mechanism exists for synthesizing these particles within chloroplast membranes. Nanoceria interchange oxidation states between Ce^{3+} and Ce^{4+}, forming oxygen vacancies with dangling Ce^{3+} bonds[28] (Supplementary Fig. 2a,b). Lattice strains promote the formation of defect sites with regeneration of the Ce^{3+} oxidation state via redox cycling reactions[28]. Thus, nanoceria are well positioned to catalytically scavenge hydroxyl and superoxide radicals at chloroplast sites of generation via the following reactions:

$$Ce^{3+} \longleftrightarrow Ce^{4+} + e^-$$

$$Ce^{3+} + OH^\bullet \longrightarrow Ce^{4+} + OH^-$$

$$Ce^{4+} + O_2^{\bullet-} \longrightarrow Ce^{3+} + O_2$$

Previous studies demonstrated the potential of dextran-wrapped nanoceria as ROS scavengers for isolated chloroplasts[2] and

microalgae[29] despite their inability to move through lipid bilayers and cell walls. According to our uptake mechanism, dextran-wrapped nanoceria do not interact with the chloroplast membrane owing to their neutral zeta potential[30]. We reasoned that nanoceria particles with a high negative or positive zeta potential will localize within the chloroplast envelope. Here we show confocal images demonstrating that negatively charged poly(acrylic acid) nanoceria (PAA–NC; ref. 30) co-localize with chlorophyll molecules inside isolated chloroplasts (Fig. 3h). The proposed mechanism of chloroplast nanoparticle uptake also extends to a new nanomaterial of SWNTs conjugated with PAA–NC via carbodiimide chemistry (SWNT–NC). In brief, SWNT–NC were synthesized from HiPCO SWNTs (Unidym) suspended with a 30-base (dAdT) sequence of ssDNA (AT$_{15}$) functionalized with amino groups at the 5′ end (Integrated DNA Technologies). The PAA–NC and 5′ amino-ss(AT)$_{15}$–SWNTs were conjugated with a zero crosslink carbodiimide agent N-ethyl-N'-(3-dimethylaminopropyl) carbodiimide hydrochloride (EDAC; Sigma Aldrich). The solution was purified from reagents by bench-top centrifugation using a 100 K Amicon membrane (Millipore). Fourier-transform infrared spectroscopy indicates the formation of amide bonds between amino groups at the 5′ end of DNA-coated ss(AT)$_{15}$–SWNTs and the hydroxyl groups of PAA–NC (Supplementary Fig. 2c). The size of SWNT–NC complexes determined by atomic force microscopy and transmission electron microscopy (TEM) was in the range of several hundred nanometres in length and 4–7 nm in height (Supplementary Fig. 2d,e). TEM image analysis showed that 55 ± 7% SWNTs were conjugated with 4 ± 2 nanoceria particles on average (Fig. 3i). The conjugation of NC with SWNTs by carbodiimide chemistry produced individual SWNT–NC complexes with characteristic peaks in near-infrared fluorescence (Supplementary Fig. 3a,b). These SWNT–NC complexes were able to penetrate the chloroplast envelope and assembled within photosynthetic machinery (Fig. 3j and Supplementary Fig. 4a,b). The nanoparticles localized in proximity to the chloroplast thylakoid membranes and stroma in which the light and carbon reactions of photosynthesis occur, respectively. Chloroplast intactness after being interfaced with SWNTs and SWNT–NC remained unchanged at approximately 85% (Supplementary Fig. 5).

SWNT augmentation of chloroplast photosynthetic activity

Enhanced and extended photosynthetic activity by passive assembly of extracted chloroplasts with SWNT–NC was shown by higher reduction rates of the electron acceptor dye dichlorophenolindophenol (DCPIP; Fig. 4a). DCPIP intercepts electrons transported from photosystem II to photosystem I in the chloroplast photosynthetic machinery[31]. PAA–NC interfaced with chloroplasts had an optimum concentration at 8 μM, showing slightly higher photosynthetic activity for the initial 3.5 h followed by complete deactivation of photosynthetic electron transport after 6 h. However, a control sample of DCPIP and PAA–NC in buffer showed similar reduction indicating that PAA–NC did not significantly improve photosynthetic activity (Supplementary Fig. 6). SWNT–NC particles had the strongest effect on photosynthetic activity with more than three times higher chloroplast DCPIP reduction than the control after 6 h. This suggests that the presence of SWNT, not NC, may be the cause of enhanced photosynthetic activity for SWNT–NC, instead of ROS scavenging. Although it seems that the observed scavenging of ROS did not significantly improve photosynthetic activity, it may be beneficial for other processes, such as carbon-fixation reactions. Extracted chloroplast photosynthesis was also quantified by measuring the yield of chlorophyll fluorescence using a MINI-PAM photosynthesis analyser (WALZ). Maximum electron transport rates of light-adapted chloroplasts were significantly increased

by 49% with SWNTs at 2.5 mg l^{-1} (Fig. 4b). Remarkably, SWNTs also enhance the light reactions of photosynthesis of chloroplasts inside leaves *in vivo*. Leaves infiltrated with 2.5 and 5 mg l^{-1} of SWNTs showed a 27% and 31% increase in maximum electron-transport rates over leaves without SWNTs, respectively (Fig. 4b). Rates of electron transport were also higher with photosynthetic active radiations above 100 µmol m^{-2} s^{-1} in leaves with SWNTs at 5 mg l^{-1}, but no effect was observed in extracted chloroplasts (Fig. 4c and Supplementary Fig. 7a,b). The difference in this behaviour is probably due to variations in optimum light levels for photosynthesis in extracted chloroplasts versus chloroplasts in leaves. Together our results indicate that SWNTs are able to enhance solar energy conversion of chloroplasts both *in vivo* and *ex vivo*.

One possible explanation for the enhancement of photosynthetic activity by SWNTs is electron transfer between SWNTs and chloroplasts. SWNTs have been reported to generate a photoelectrochemical current on dynamic assembly with extracted reaction centres and nanodisc lipids[32]. Electron transfer between carbon nanotubes and photosynthetic machinery has been demonstrated in many studies[33], including recently between nanotubes and spinach thylakoids[34]. Thus, the assembly of SWNTs within the photosynthetic machinery may modify the chloroplast absorption profile by increasing light energy capture in ultraviolet, green and near-infrared ranges of the spectrum (Fig. 4d). Semiconducting SWNTs are then able to convert this absorbed light into excitons that can be transferred to the chloroplast electron transport chain (Fig. 4e). To confirm this mechanism, the photosynthetic activity of extracted chloroplasts assembled with separated, metallic SWNTs (m-SWNTs) and unseparated HiPCo SWNTs (Unidym, approximately 1/3 metallic, 2/3 semiconducting) were compared. If semiconducting SWNTs enhance light capturing, then metallic SWNTs should show less of an impact because they are not able to convert light energy to excitons. As expected, m-SWNTs showed a minimal effect on chloroplast reduction of the electron acceptor dye DCPIP over six hours (Fig. 4e). Similar trends of nanoparticle impact on chloroplast photosynthetic activity were observed at initial rates of DCPIP reduction (Supplementary Fig. 6a–d). Different concentrations of the mix of HiPCo SWNTs had the same increase in photosynthetic activity. However, increasing concentrations of m-SWNTs decreased the reduction of DCPIP relative to chloroplasts without nanoparticles from one to six hours. This negative effect of m-SWNTs on chloroplast photosynthetic activity probably occurs because m-SWNTs absorb light that chloroplasts could otherwise have captured (Supplementary Fig. 8), but m-SWNTs are unable to transfer any of this energy to the electron transport chain.

Nanoparticle enhancement of chloroplast ROS scavenging

PAA–NC and SWNT–NC localized inside extracted chloroplasts significantly decrease the ROS concentration, as shown by the conversion of the dye H$_2$DCFDA to its fluorescent form DCF (Fig. 4f). H$_2$DCFDA oxidation to DCF by a range of free radicals such as hydrogen peroxide, superoxide, NO and peroxidases has been applied to monitor ROS generated by extracted chloroplasts[35]. Under continuous illumination for six hours, chloroplasts interfaced with 6 µM PAA–NC showed a substantial 28.7% reduction in ROS relative to chloroplasts without nanoparticles. SWNT–NC were less effective than PAA–NC at scavenging ROS. The optimum concentration of SWNT–NC (0.5 mg l^{-1}) led to a 21.4% drop in chloroplast ROS generation. Superoxide concentrations considerably declined from 31.29 ± 1.56 µM down to 12.99 ± 0.89 µM with PAA–NC and 17.62 ± 2.57 µM with SWNT–NC after two hours. Scavenging of short-lived ROS, such as superoxide, is facilitated by the proximity of nanoparticles to the

sites of ROS generation near the thylakoid membranes, providing a quick pathway for superoxide radicals to react with nanoceria Ce^{3+} dangling bonds (Fig. 4g). Whereas chloroplast superoxide scavenging by 17 µM PAA–NC declined over time, other PAA–NC concentrations and all SWNT–NC concentrations maintained significantly lower levels of superoxide, with 1.4 and 2.8 mg l^{-1} SWNT–NC having the maximum impact.

SWNT NO sensing inside extracted chloroplasts and leaves

We have previously designed and characterized ss(AT)$_{15}$–SWNTs as fluorescent detectors of nitric oxide[36] (NO). NO is a key signalling molecule found in chloroplasts[37] and also an environmental pollutant. Our new-found ability to localize ss(AT)$_{15}$–SWNTs in chloroplasts offers an opportunity to embed this real-time sensor of NO within the photosynthetic apparatus to monitor and control the degradation rate. Here, we demonstrate the potential for NO detection in plants by ss(AT)$_{15}$–SWNTs (Fig. 4h,i). We found that all SWNT chiralities with a peak of emission above 1,100 nm undergo a strong quenching in near-infrared fluorescence in the presence of dissolved NO in both extracted chloroplasts and leaves *in vivo*. We show real-time imaging of free-radical diffusion in a living plant using a SWNT-based sensor (Fig. 4j,k and Supplementary Video). Near-infrared images of the leaf lamina confirmed a steep reduction in SWNT sensor intensity on perfusion of dissolved NO (Fig. 4l). The development of nanobionic leaves with new sensing capabilities has the potential to create plant biochemical detectors for both endogenous signalling molecules and exogenous environmental compounds. Recent progress in separation of single-chirality SWNTs (ref. 38) will enable the development of more robust sensors with multimodal responses for *in vivo* applications[39].

Conclusions

Nanotechnology has the potential to enable new and enhanced functional properties in photosynthetic organelles and organisms for the enhancement of solar energy harnessing and biochemical sensing. The development of nanobionic plants is facilitated by the passive assembly of high-zeta-potential nanomaterials within the chloroplast photosynthetic machinery via kinetic trapping by lipid exchange. Semiconducting SWNTs delivered by this spontaneous mechanism have the potential for increasing chloroplast carbon capture by promoting chloroplast solar energy harnessing and electron-transport rates. Future studies will explore the effect of nanoparticle assemblies on the carbon reactions of photosynthesis and chloroplast sugar export. Nanomaterial enhancement of isolated chloroplast stability to free radicals and higher photosynthetic efficiencies opens the possibility of creating hyperstable synthetic materials that grow and repair themselves using sunlight, water and carbon dioxide. SWNT real-time sensing of NO in extracted chloroplasts and leaves could also be extended to detect a wide range of plant signalling molecules and exogenous compounds such as pesticides, herbicides and environmental pollutants. Nanomaterials offer a promising way to engineer plant function, but the absorption, transport and distribution of nanoparticles within photosynthetic organisms remain poorly understood. This nanobionics approach to engineer plant function will lead to a new research field at the interface of nanotechnology and plant biology.

Methods

Plant material. Chloroplasts were isolated from commercially available baby spinach leaves (*Spinacia oleraceae* L.) as described previously[1] with modifications (Supplementary Methods). A 90% chloroplast intactness was determined by ferricyanide photoreduction with and without osmotic shock as in ref. 40. Chlorophyll concentration was determined according to ref. 41. Wild-type var. Col. *Arabidopsis thaliana* plants between 4 and 6 weeks old were sampled for leaf nanoparticle uptake and electron transport rates. Plants were grown in propagation liner trays (Nursery supplies) with a soil mixture of Fafard Mix#3B

maintained at water field capacity. Ambient temperature was 25°C day/19°C night during a 13 h photoperiod. Leaf chlorophyll content was measured with a SPAD meter (Minolta, SPAD 502).

Nanomaterial uptake by isolated chloroplasts. SWNT chloroplast uptake videos were recorded in an AxioVision inverted microscope (Zeiss, Axiovert 200) coupled to a 2D InGaAs CCD (charge-coupled device) array (OMA-V 2D, Princeton Instruments). Raman spectroscopy 3D maps were acquired in a confocal Raman spectrometer HR-800 (Horiba BY). The PAA–NC confocal images were taken in a Zeiss LSM 710 NLO microscope. Nanoceria were labelled via carbodiimide reaction with Alexa Fluor 405 Cadaverine (Invitrogen). A FEI Technai Spirit TEM microscope at 80 kV was used to image chloroplast uptake of the SWNT–NC complex. Cerium analysis by inductively coupled mass spectroscopy (ICP-MS) was performed on chloroplasts after purification from free SWNT–NC. Samples were characterized by ICP-MS at Elemental Analysis under project number 6197-12.

Leaf infiltration with SWNTs for near-infrared microscopy and spectroscopy. Leaves of *Arabidopsis thaliana* were infiltrated with 100 µl of ss(AT)$_{15}$–SWNTs as in ref. 42. Whole-leaf near-infrared imaging was performed on a CRi Maestro (PerkinElmer). Leaf cross-sections and whole leaves were also imaged in the near-infrared by an Axiovision Zeiss inverted microscope (Zeiss, Axiovert 200) with a 2D InGaAs CCD array (OMA-V 2D, Princeton Instruments) using a 785 nm Invictus photodiode laser excitation (Kaiser). Leaf bright-field images were taken with a Zeiss bright-field camera (Zeiss, Axio-Cam Mrm). Chloroplast fluorescence was imaged with a 658 nm 200 mW diode-pumped solid-state laser (CrystaLaser, RCL-100-660) and a band-pass filter 700–750 nm (Chroma).

For spectrometry of leaves with infiltrated SWNTs, the Axiovision Zeiss inverted microscope (Zeiss, Axiovert 200) was coupled to an InGaAs array detector (OMA-V, Princeton Instruments) through an Acton SP-2500 spectrograph (Princeton Instruments). Infiltrated SWNTs were excited with a 785 nm Invictus photodiode laser excitation (Kaiser) through the leaf lamina. Images were acquired at a frame rate of 2 Hz, and spectra were recorded with a 10 s exposure time. The near-infrared fluorescence of SWNTs was not detected in control leaves treated with only infiltration medium (Supplementary Fig. 1a–d). Control leaves had a background signal up to 1,025 nm and 2,000 cm^{-1} in near-infrared fluorescence and Raman spectra, respectively. Raman spectra were collected in an HR-800 spectrometer (Horiba BY) using a 785 nm laser source with a ×10 objective at 2 cycles of 5 s each.

Nanoceria scavenging of ROS. Chloroplast (approximately 0.01 mg Chl ml^{-1}) ROS scavenging by nanoparticles was quantified by the conversion of the membrane permeant 2′,7′-dichlorodihydrofluorescein diacetate (H$_2$DCFDA, 0.6 mg ml^{-1}) to the fluorescent 2′,7′-dichlorofluorescein (DCF; ref. 35). The effect of nanoparticles on superoxide concentration was determined by the reduction of 2,3-bis (2-methoxy-4-nitro-5-sulphophenyl)-2H-tetrazolium-5-carboxanilide sodium salt (XTT, 0.06 mg ml^{-1}) dye (Sigma Aldrich) in the presence of superoxide as in previous studies on plant cells[43,44]. We confirmed that the reduction of XTT responds to chloroplast superoxide concentration by incubating chloroplasts with superoxide dismutase (SOD), a well-known superoxide scavenger (Supplementary Fig. 9).

Extracted chloroplast and leaf photosynthesis. Photosynthetic activity was monitored in isolated chloroplasts (approximately 0.01 mg Chl ml^{-1}) in sucrose buffer by measuring the change from initial absorbance at 600 nm of the electron acceptor dye dichloroindophenol (DCPIP, 0.034 mg ml^{-1}) with an extinction coefficient of 21.7 mM^{-1} cm^{-1} (ref. 31). The effect of SWNT and SWNT–NC alone on DCPIP in buffer was not significant relative to nanoparticles interfaced with chloroplasts (Supplementary Fig. 6). Chloroplasts were illuminated with a light intensity of approximately 200 µmol m^{-2} s^{-1} photosynthetic active radiation (40 W m^{-2}) with a light-emitting diode flood lamp FL-70W (LED wholesalers). Cerium nitrate treatments were performed as a control at the same concentrations of PAA–NC. Cerium did not influence chloroplast photosynthetic activity (Supplementary Fig. 11c). Leaf electron transport rates were assessed by measuring the yield of chlorophyll fluorescence with a MINI-PAM photosynthesis yield analyser (WALZ). Light absorbed by chlorophyll pigments can be used for photochemistry and excess energy is converted into heat or re-emitted as fluorescence. By measuring the yield of chlorophyll fluorescence, information about these competing processes can be quantified to calculate the rate of electron transport, an indicator of the light reactions of photosynthesis[45].

Optical sensing of NO in chloroplast *ex vivo* and leaves *in vivo*. For NO quenching experiments, isolated chloroplasts (0.01 mg Chl ml^{-1}) were suspended in 200 µl solution of ss(AT)$_{15}$–SWNTs (5 mg l^{-1}) in water for 15 min. The near-infrared fluorescence spectrum was collected as explained above in a range of 1,150 to 1,450 nm with a 10 s exposure time under a 785 nm laser excitation. Then 10 µl of NO solution was added and the measurements were repeated. For leaves, a region of interest within the leaf lamina was found with several SWNT fluorescence sources. Small incisions were made adjacent to the SWNT regions of interest to allow NO internalization. A 20 µl volume of a dissolved NO solution was added to the leaf incision and the SWNT intensity at the predetermined regions of interest was imaged for 500 s and spectra collected at 10 s exposure time as explained above. For control experiments, the process was repeated by adding H$_2$O instead of NO to the extracted chloroplasts and the leaf lamina (Supplementary Fig. 10). Image processing was accomplished by monitoring the peak-intensity profile of SWNT regions of interest as a function of time for the duration of the movie. SWNT peak intensity did not change substantially after addition of H$_2$O.

References

1. Weise, S. E., Weber, A. P. M. & Sharkey, T. D. Maltose is the major form of carbon exported from the chloroplast at night. *Planta* **218,** 474–482 (2004).
2. Boghossian, A. A. *et al.* Application of nanoparticle antioxidants to enable hyperstable chloroplasts for solar energy harvesting. *Adv. Energy Mater.* **3,** 881–893 (2013).
3. Trench, R. K., Boyle, J. E. & Smith, D. C. The association between chloroplasts of *Codium fragile* and the mollusc *Elysia viridis*. I. characteristics of isolated *Codium* chloroplasts. *Proc. R. Soc. B Biol. Sci.* **184,** 51–61 (1973).
4. Rumpho, M. E., Summer, E. J. & Manhart, J. R. Solar-powered sea slugs. Mollusc/algal chloroplast symbiosis. *Plant Physiol.* **123,** 29–38 (2000).
5. Choe, H. & Thimann, K. The senescence of isolated chloroplasts. *Planta* **121,** 201–203 (1974).
6. Green, B. J., Fox, T. C. & Rumpho, M. E. Stability of isolated algal chloroplasts that participate in a unique mollusc/kleptoplast association. *Symbiosis* **40,** 31–40 (2005).
7. Neuhaus, H. E. & Schulte, N. Starch degradation in chloroplasts isolated from C3 or CAM (crassulacean acid metabolism)-induced Mesembryanthemum crystallinum L. *Biochem. J.* **318,** 945–953 (1996).
8. Edelman, M. & Mattoo, A. K. D1-protein dynamics in photosystem II: The lingering enigma. *Photosynth. Res.* **98,** 609–620 (2008).
9. Schmitz-Linneweber, C. *et al.* The plastid chromosome of spinach (*Spinacia oleracea*): complete nucleotide sequence and gene organization. *Plant Mol. Biol.* **45,** 307–315 (2001).
10. Marín-Navarro, J., Manuell, A. L., Wu, J. P. & Mayfield, S. Chloroplast translation regulation. *Photosynth. Res.* **94,** 359–374 (2007).
11. Bolton, J. R. & Hall, D. Photochemical conversion and storage of solar energy. *Annu. Rev. Energy* **4,** 353–401 (1979).
12. Zhu, X.-G., Long, S. P. & Ort, D. R. Improving photosynthetic efficiency for greater yield. *Annu. Rev. Plant Biol.* **61,** 235–261 (2010).
13. Blankenship, R. E. *et al.* Comparing photosynthetic and photovoltaic efficiencies and recognizing the potential for improvement. *Science* **332,** 805–809 (2011).
14. Wilhelm, C. & Selmar, D. Energy dissipation is an essential mechanism to sustain the viability of plants: The physiological limits of improved photosynthesis. *J. Plant Physiol.* **168,** 79–87 (2011).
15. Scholes, G. D., Fleming, G. R., Olaya-Castro, A. & van Grondelle, R. Lessons from nature about solar light harvesting. *Nature Chem.* **3,** 763–774 (2011).
16. Han, J-H. *et al.* Exciton antennas and concentrators from core–shell and corrugated carbon nanotube filaments of homogeneous composition. *Nature Mater.* **9,** 833–839 (2010).
17. Zhang, J. *et al.* Single molecule detection of nitric oxide enabled by d(AT)(15) DNA adsorbed to near infrared fluorescent single-walled carbon nanotubes. *J. Am. Chem. Soc.* **20,** 567–581 (2010).
18. Shi, X., von dem Bussche, A., Hurt, R. H., Kane, A. B. & Gao, H. Cell entry of one-dimensional nanomaterials occurs by tip recognition and rotation. *Nature Nanotech.* **6,** 714–719 (2011).
19. Pogodin, S., Slater, N. K. H. & Baulin, V. a. Surface patterning of carbon nanotubes can enhance their penetration through a phospholipid bilayer. *ACS Nano* **5,** 1141–1146 (2011).
20. Chen, J., Patil, S., Seal, S. & McGinnis, J. F. Rare earth nanoparticles prevent retinal degeneration induced by intracellular peroxides. *Nature Nanotech.* **1,** 142–150 (2006).
21. Soll, J. & Schleiff, E. Protein import into chloroplasts. *Nature Rev. Mol. Cell Biol.* **5,** 198–208 (2004).
22. Pogodin, S. & Baulin, V. a. Can a carbon nanotube pierce through a phospholipid bilayer? *ACS Nano* **4,** 5293–5300 (2010).

23. Leheny, E. A. & Theg, S. M. Apparent inhibition of chloroplast protein import by cold temperatures is due to energetic considerations not membrane fluidity. *Plant Cell* **6,** 427–437 (1994).
24. Ma, X. *et al.* Single-walled carbon nanotubes alter cytochrome *c* electron transfer and modulate mitochondrial function. *ACS Nano* **6,** 10486–10496 (2012).
25. Block, M. a, Douce, R., Joyard, J. & Rolland, N. Chloroplast envelope membranes: a dynamic interface between plastids and the cytosol. *Photosynth. Res.* **92,** 225–244 (2007).
26. Liu, Q. L. *et al.* Carbon nanotubes as molecular transporters for walled plant cells. *Nano Lett.* **9,** 1007–1010 (2009).
27. Lim, P. O., Kim, H. J. & Nam, H. G. Leaf senescence. *Annu. Rev. Plant Biol.* **58,** 115–136 (2007).
28. Deshpande, S., Patil, S., Kuchibhatla, S. V. & Seal, S. Size dependency variation in lattice parameter and valency states in nanocrystalline cerium oxide. *Appl. Phys. Lett.* **87,** 133113 (2005).
29. Sicard, C. *et al.* CeO₂ nanoparticles for the protection of photosynthetic organisms immobilized in silica gels. *Chem. Mater.* **23,** 1374–1378 (2011).
30. Asati, A., Santra, S., Kaittanis, C. & Perez, J. M. Surface-charge-dependent cell localization and cytotoxicity of cerium oxide nanoparticles. *ACS Nano* **4,** 5321–5331 (2010).
31. Lonergan, T. A. & Sargent, M. L. Regulation of the photosynthesis rhythm in Euglena gracilis CS1-75. *Plant Physiol.* **64,** 99–103 (1979).
32. Ham, M-H. *et al.* Photoelectrochemical complexes for solar energy conversion that chemically and autonomously regenerate. *Nature Chem.* **2,** 929–936 (2010).
33. Boghossian, A. A., Ham, M.-H., Choi, J. H. & Strano, M. S. Biomimetic strategies for solar energy conversion: a technical perspective. *Energy Environ. Sci.* **4,** 3834–3843 (2011).
34. Calkins, J. O., Umasankar, Y., O'Neill, H. & Ramasamy, R. P. High photo-electrochemical activity of thylakoid–carbon nanotube composites for photosynthetic energy conversion. *Energy Environ. Sci.* **6,** 1891–1900 (2013).
35. Mubarakshina, M. M. *et al.* Production and diffusion of chloroplastic H₂O₂ and its implication to signalling. *J. Exp. Bot.* **61,** 3577–3587 (2010).
36. Kim, J-H. *et al.* The rational design of nitric oxide selectivity in single-walled carbon nanotube near-infrared fluorescence sensors for biological detection. *Nature Chem.* **1,** 473–481 (2009).
37. Wilson, I. D., Neill, S. J. & Hancock, J. T. Nitric oxide synthesis and signalling in plants. *Plant. Cell Environ.* **31,** 622–631 (2008).
38. Tvrdy, K. *et al.* A kinetic model for the deterministic prediction of gel-based carbon nanotube separation. *ACS Nano* **7,** 1779–1789 (2013).
39. Heller, D. A. *et al.* Multimodal optical sensing and analyte specificity using single-walled carbon nanotubes. *Nature Nanotech.* **4,** 114–120 (2009).
40. Lilley, R. M., Fitzgerald, M. P., Rienits, K. G. & Walker, D. A. Criteria of intactness and the photosynthetic activity of spinach chloroplast preparations. *New Phytol.* **75,** 1–10 (1975).
41. Arnon, D. Copper enzymes in isolated chloroplasts polyphenoloxidase in *Beta vulgaris. Plant Physiol.* **24,** 1–16 (1949).
42. Huang, X. *et al.* Magnetic virus-like nanoparticles in *N benthamiana* plants: a new paradigm for environmental and agronomic biotechnological research. *ACS Nano* **5,** 4037–4045 (2011).
43. Jiang, M. Water stress-induced abscisic acid accumulation triggers the increased generation of reactive oxygen species and up-regulates the activities of antioxidant enzymes in maize leaves. *J. Exp. Bot.* **53,** 2401–2410 (2002).
44. Able, A., Guest, D. & Sutherland, M. Use of a new tetrazolium-based assay to study the production of superoxide radicals by tobacco cell cultures challenged with avirulent zoospores of *Phytophthora parasitica* var nicotianae. *Plant Physiol.* **117,** 491–499 (1998).
45. Maxwell, K. & Johnson, G. N. Chlorophyll fluorescence—a practical guide. *J. Exp. Bot.* **51,** 659–668 (2000).

Author contributions

J.P.G. and M.S.S. conceived experiments and wrote the paper. J.P.G., M.P.L., S.M.F., T.P.M. and N.M.I. performed experiments and data analysis. A.A.B., F.S, A.J.H., N.F.R. and J.A.B. assisted in experiments and analysis.

Additional information

Supplementary information is available in the online version of the paper. Reprints and permissions information is available online at www.nature.com/reprints. Correspondence and requests for materials should be addressed to M.S.S.

Plant nanobionics approach to augment photosynthesis and biochemical sensing

Juan Pablo Giraldo, Markita P. Landry, Sean M. Faltermeier, Thomas P. McNicholas, Nicole M. Iverson,
Ardemis A. Boghossian, Nigel F. Reuel, Andrew J. Hilmer, Fatih Sen, Jacqueline A. Brew and Michael S. Strano

In the version of this Article originally published, in Fig. 4k, the scale bar should have been 16 µm, and in the sentence beginning "Leaves assembled with CoMoCAT…" the characteristic fluorescence peak for the (6,5) chirality should have read '(980–1,000 nm)'. These errors have now been corrected in the online versions of the Article.